VALERI 2000, Romilly Site (06/05/2000-06/09/2000):

Marie WEISS

Participants: N. Bruguier, O. Marloie, M. Weiss (INRA Avignon, Bioclimatologie)
L. Bonneau de Beaufort, D. Allard (INRA Avignon, Biométrie)

Table of Contents

A. Introduction

The objective of the VALERI project (VALidation of European Remote Sensing Instruments) is to develop a validation site network for the level3 products (biophysical variables) of European large swath sensors. For each validation site, one needs to provide maps of measured biophysical variables at different spatial resolutions (from 250m to 7km) and for each site. During this campaign , a *licor* LAI2000 as well as an *hemiview*, allowed to obtain ground measurements of leaf area index (LAI) and gap fraction ($P_o(\theta)$ in 5 viewing directions (zenithal angle θ of 7°, 23°, 38°, 53°, 68°). The use of those instruments requires diffuse radiation conditions that can be only obtained at sunrise or sunset. Due to dewy crops and drops of water on the LAI2000 lens, measurements were performed in the evening. Considering the site size (10km by 10km), a sampling strategy, as well as an associated method to extrapolate the measurements to the entire site, have been defined. 50 field acquisitions, associated to GPS positions, were thus performed. To allow atmospheric correction on satellite images, aerosol optical thickness was measured using a sunphotometer during an entire day (06/08/2000).

Romilly/Seine is located in the Seine Valley between the towns of Provins et Troyes (France). The site is an intensive agricultural area of 10km by 10km (Table 1) composed of early crops (wheat, barley, pea, alfalfa, colza, hemp, poppy) and late crops (maize, sugar beet, sunflower, potatoes). It also includes few urban and woody zones. Figure 1 is an image of the site acquired with Spot4 in MAY 2000.

	Latitude Longitude	**Lambert I Nord, Est**
Upper Left	48°29'47.98 N 3°44'18.85 E	1089650 N 713590 E
Lower Right	48°24'18.00 N 3°52'15.92 E	1079650 N 703590 E

Table 1: Romilly site location.

B. Sampling Strategy and protocol of measurement in each plot

The image acquired with SPOT4 in May 2000 allowed to define a simple sampling strategy by dividing the area into 49 1km-size sub-areas. In each sub-area, at least one measurement was performed. The field was chosen so that it characterizes the main crop in the sub-area and by taking into account that each crop should be sampled in proportion to its total size in the whole area.

Except for colza, 12 local cross-shaped measurements composed of one above canopy and four below acquisitions for LAI2000 and one above canopy picture (Hemiview camera) are performed in the 50 fields. Measurements are distant from 4m and thus, each part of the cross is 20m long (Fig.2). In case or row crops, the 20m cross is always placed transversely to the rows. The *GPS* positioning is achieved at the center of the cross, with a 1m accuracy in 95% of the points. Location was performed by averaging the *GPS* measurements over 1mn. No differential post processing was performed. Georeferencement is carried out in a Lambert I projection described in table 2 . The measurements were also performed at more than 40m from the field edges, except for Colza crops that were too dense to penetrate inside. For Colza, measurements have been acquired on the field edge (no cross shape).

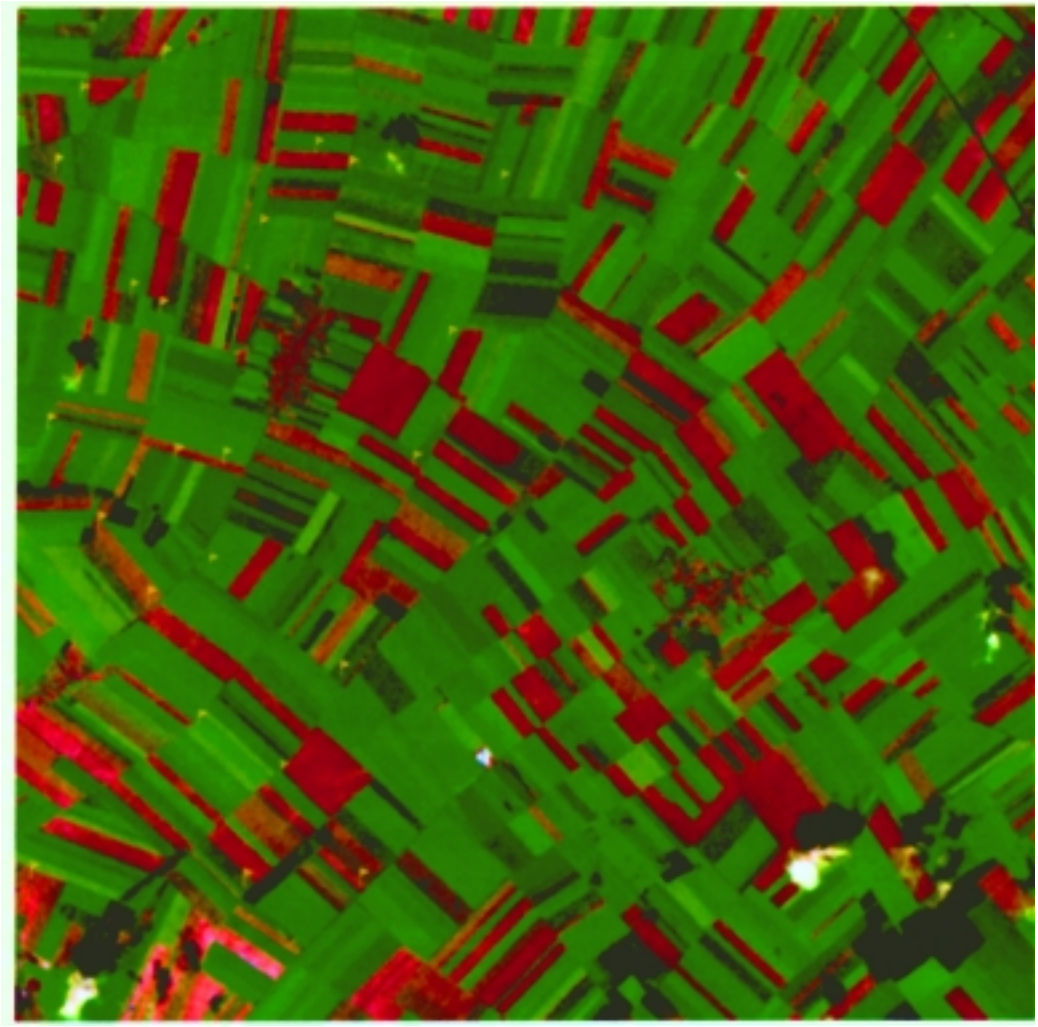

Figure 1. SPOT4 image of the Romilly Site in May 2000 (10kmx10km). Woody areas are represented in black, bare soils in red and developed crops in green.

Datum	Clarke 1880
1st standard Parallel	48°35'64.682" N
2nd standard Parallel	50°23'45.282" N
Coordinates of Origin	49°30'00'' N 2°20'14.025" E
False northing	600 000 m
False easting :	200 000 m

Table 2: Description of Lambert I projection characteristics.

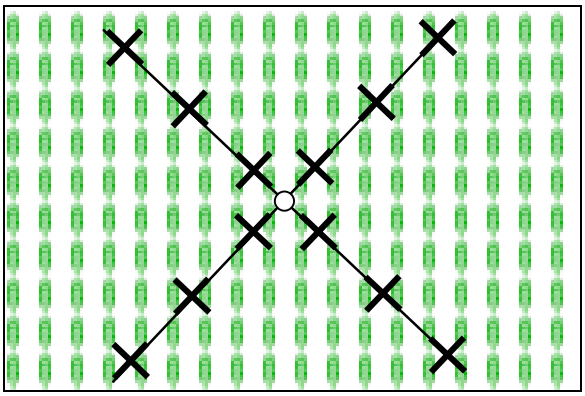

Figure 2. Protocol of ground measurements in one field. Bold crosses correspond to LAI2000 acquisitions (1 above and four below) or one *Hemiview* hemispherical pictures. The central point coincide with the *GPS* positioning.

C. Raw data: file names and format (directory RawData)

ASCII file *Positions.txt* assign the name, Julian day of measurement, *GPS* positioning (East and North Lambert I coordinates and altitude) and the instrument (*LAI2000* or *Hemiview*) used for each field. Four LAI2000 were used: two provided by INRA Bioclimatologie Avignon (*N* is a number) and two provided by INRA Bioclimatologie Bordeaux and CIRAD (*N* is a letter). Each instrument was calibrated using the parameters provided by Licor. For *Hemiview* acquisitions *N* is a letter. Table 3 gives an overview of the 50 acquisitions.

	Field	DOY	Easting (m)	Northing (m)	Altitude (m)	Instru	Plot Nb	Orientation and Notes
ALFALFA	ALF1	158	703947	1087761	80	0	12	NO/SE
	ALF2	160	709954	1086762	101	0	12	
	ALF3	161	703722	1080791	157	0	12	Young crop
	ALFA	158	707924	1080394	146	0	12	E/O
	ALFB	160	709006	1083606	108	0	12	Heterogeneous field
	ALFC	161	711108	1088258	111	0	12	Homogeneous
BARLEY	BAR1	159	705355	1082283	125	0	12	Direct radiation possible
	BAR2	159	713316	1081829	103	0	12	
	BAR3	159	711800	1080494	131	0	12	Quite yellow, lodged
	BAR4	160	707806	1086065	93	0	12	
	BAR5	161	704191	1088469	84	0	12	Yellow
	BARA	159	712742	1084149	97	0	12	
	BARB	161	703874	1085209	99	0	10	Young crop
	BARC	161	710219	1088939	104	0	12	
COLZA	COL1	159	706792	1087779	98	0	12	N/S
	COLA	158	708431	1080768	129	0	12	N/S
	COLB	158	709661	1080570	132	0	12	E/O
HEMP	HEMA	158	710144	1081136	119	0	11	
	HEMB	159	704373	1084231	129	0	12	Direct radiation possible
	HEMC	161	708421	1080730	138	0	12	Dense
	HEMD	161	709594	1085994	115	0	12	
MAIZE	MAI1	161	704409	1082686	107	1	12	
PEA	PEA1	161	705807	1080709	158	0	12	Direct radiation possible
	PEAA	159	704683	1086527	90	0	12	Direct radiation possible
	PEAB	159	706749	1082761	131	0	12	Direct radiation possible
	PEAC	159	712251	1083733	98	0	12	
	PEAD	159	712510	1085808	92	0		
	PEAE	161	709178	1081392	133	0	12	Dense
	PEAF	161	708292	1081031	134	0	12	

POPPY	POP1	159	711292	1081153	115	0	12	Wet conditions
	POPA	159	704865	1083499	125	0	13	Wet conditions
	POPB	161	709016	1085097	122	0	12	
POTATOES	POT1	157	707925	1085348	104	1	12	E/O
	POT2	158	708956	1086558	90	1	11	E/O
	POT4	158	713129	1087747	98	1	12	N/S
	POT5	159	712430	1080576	122	1	12	
SUN FLOWER	SUF1	157	712443	1082602	105	0	12	SO/NE
	SUF2	157	707456	1084831	108	0	12	SO/NE
SUGAR BEET	SUG1	157	706940	1080714	-	0	12	SE/NO
	SUG2	157	705595	1084868	106	0	12	E/O
	SUG3	157	706487	1087932	95	0	12	E/O
	SUG4	158	711292	1088775	98	0	12	N/S
	SUG5	158	711201	1086780	110	0	11	SO/NE
WHEAT	WHE1	159	705955	1087160	95	0	12	NE/SO (no spike)
	WHE2	159	713275	1080939	126	0	12	No spike
	WHE3	160	708311	1087598	76	0	12	No spike
	WHE4	161	705000	1088832	88	0	12	No spike
	WHEA	159	704968	1086351	100	0	12	Spikes Direct radiation possible
	WHEB	159	705465	1083821	129	0	12	Direct radiation possible
	WHEC	159	706156	1081781	143	0	12	Direct radiation possible
	WHED	159	711703	1083167	103	0	11	
	WHEE	160	708562	1082044	115	0	12	No spike
	WHEF	160	708751	1083419	116	0	12	spikes
	WHEG	160	705638	1084830	100	0	12	spikes, homogeneous
	WHEH	161	705122	1084904	109	0	12	No spike Direct radiation possible

Table 3: Description of Romilly Site ground measurements. Column *instru* is 0 for *LAI2000* and 1 for *Hemiview*

Each LAI2000 ASCII file is labeled as *FFFN_day*.dat, where *FFFN* is the first 3 letters of the crop type (except for sunflower *SUF*), *N* characterizes each field of a same crop and is a letter or a number depending on the LAI2000 instrument used for the data acquisitions, and *day* is the Julian day number. For one field, the 12 *LAI2000* files are grouped in one. A *LAI2000* file correspond to LAI2000 software output s(figure 3). See *Licor* user reference guide.
Hemispherical pictures are in a *jpeg* format, with the same name format as LAI2000 files.

```
 FILE  DATE   TIME      1        4      LAI    SEL   DIFN   MTA    SEM SMP
    7  05 JUN 18:04:45  BET1     1     1.78   0.23  0.226    39      1   4

ANGLES   0.0  23.00  38.00  53.00  68.00
CNTCT# 1.718  1.275  1.003  0.859  0.734
STDDEV 1.262  0.466  0.274  0.285  0.136
DISTS  1.008  1.087  1.270  1.662  2.670
GAPS   0.178  0.251  0.281  0.241  0.141

A  1 18:11:25  9.745  9.176  8.608  7.791  6.776
B  2 18:11:27  1.320  2.400  4.022  2.463  0.997
B  3 18:11:31  0.261  1.467  2.033  1.202  0.688
B  4 18:11:34  8.327  5.164  2.634  3.532  1.695
B  5 18:11:39  3.105  1.532  1.573  1.170  0.718
```

Figure 3. Example of LAI2000 software output file.

D. LAI2000 Data Processing

The LAI2000 instrument measures the fraction of diffuse incident radiation (or transmittance $T(\theta_v)$) that passes through a plant canopy for a given view zenith angle (θ_v), assuming that the foliage is azimuthally randomly oriented. $T(\theta_v)$ is the ratio between the below-canopy and the above-canopy measurement. LAI2000 computations are based on three assumptions :

- Black foliage (under 490nm)
- Foliage elements are small compared to the area of view of each ring detector
- Foliage is azimuthally randomly oriented.

Although no real canopy conforms exactly to these assumptions, the model still works.

Errors can be observed when below measurement is higher than the above one, when no bare soil is observed. They can be due to :

- An operator mis-manipulation : for example the operator is not back to the sun
- Some clouds are passing through the sky when the operator takes the above measure, and no cloud is present when the below measurement takes place.

These measurements have been normally removed from the whole data set.

When processing, the mean gap fraction per field is computed for each ring. If the decreasing of gap fraction with increasing view angle is not verified, the file is also removed.

1. LAI2000 COMPUTATIONS :

The gap fraction in the direction θ_v , $T(\theta_v)$, can be expressed as an exponential function of the path length $S(\theta_v)$, the foliage density μ (m^2 foliage canopy per m^3 canopy) and the fraction of foliage projected towards the direction θ_v , $G(\theta_v)$:

$$T(\theta_v) = \frac{below(\theta_v)}{above(\theta_v)} = \exp(-G(\theta_v)\mu S(\theta_v)) \Rightarrow K(\theta_v) = G(\theta_v)\mu = -\frac{\ln T(\theta_v)}{S(\theta_v)} \qquad \text{Eq 1}$$

$K(\theta_v)$ is the average number of contacts per unit length of travel that a probe would make passing through the canopy at zenith angle θ_v (Welles and Norman, 1991) .

a. Foliage density computation :

It is given by : $\mu = -2\int_0^{\pi/2} \frac{\ln(T(\theta_v))}{S(\theta_v)} \sin(\theta_v) d\theta_v$

In a homogeneous canopy, foliage density is related to LAI and canopy height z . The optical path length is also related to z and θ_v :

$$\begin{cases} LAI = \mu z \\ S(\theta_v) = z / \cos(\theta_v) \end{cases} \qquad \text{Eq 2}$$

Substituing this equation in Eq 1 yields :

$$LAI = -2\int \ln(T(\theta_v))\cos\theta_v \sin\theta_v d\theta_v \qquad \text{Eq 3}$$

As measurements give $T(\theta_v)$ in only five view zenith angles, the leaf area index is computed as following:

$$LAI = 2\sum_{i=1}^{5} \frac{\ln(T(\theta_{v_i}))}{S(\theta_{v_i})} W_i \qquad \text{Eq 4}$$

Where for each detector ring centered at θ_{v_i} , of length l_i , the weight W_i is $W_i = \sin\theta_{v_i} l_i$ and the path length is $S(\theta_{v_i}) = 1/\cos\theta_{v_i}$. Table 2 shows θ_{v_i} , W_i and $S(\theta_{v_i})$ values.

θ_{v_i}	W_i	$S(\theta_{v_i})$
7°	0.034	1.008
23°	0.104	1.087
38°	0.160	1.270
53°	0.218	1.662
68°	0.494	2.670

Table 4 : Parameter value for the LAI computation

b. Average Leaf Inclination Angle :

(Lang, 1986) considers a canopy in which all the leaves are oriented at zenith angle θ_l with a random azimuth distribution. The average leaf inclination angle is expressed by a 5th order polynomial of the average slope $\overline{dG(\theta_v)/d\theta_v}$:

$$\theta_l = \sum_{i=1}^{5} a_i x^i, \quad x = \overline{dG(\theta_v)/d\theta_v} \qquad \text{Eq 5}$$

The polynomial coefficients a_i are :

$$\begin{cases} a_0 = 56.81964 & a_3 = -158.6914 \\ a_1 = 46.84833 & a_4 = 522.0626 \\ a_2 = -64.62133 & a_5 = 1008.149 \end{cases}$$

$G(\theta_{v_i})$ is computed by dividing the contact frequency by the leaf area index, for the five view zenith angles. A straight line is fit to the five $G(\theta_{v_i})$ values, and the slope of that line is used to compute θ_l from equation 5. Because of the slope is important at extreme angles, θ_l is less accurately estimated for these values. The LAI2000 forces θ_l to be between 0° and 90°.

c. Diffuse non interceptance :

It is the probability that the diffuse radiation penetrating the canopy to a particular location :

$$\tau = \frac{\int_0^{\pi/2} \Gamma(\theta_v) T(\theta_v) \sin\theta_v \cos\theta_v d\theta_v}{\int_0^{\pi/2} \Gamma(\theta_v) \sin\theta_v \cos\theta_v d\theta_v}$$

The LAI2000 computes τ, assuming an isotropic diffuse radiation meaning that $\Gamma(\theta_v) = 1$. As for leaf area index, τ is estimated usinf the five transmittance neasurements.

$$\tau = \sum T(\theta_{v_i}) W_i', \text{ where } \begin{cases} W_1 = 0.066 & W_4 = 0.249 \\ W_2 = 0.189 & W_5 = 0.249 \\ W_3 = 0.247 \end{cases}$$

2. Model inversion leaf area index and average leaf angle estimation

In this part of the processing, we assume an ellipsoïdal leaf inclination angle distribution ($\zeta(\theta_l, \theta_v)$, (Campbell, 1986)), which induces all possibilities (from planophyll to erectophyll leaves). The monodirectional gap fraction can be expressed as an exponential law of the LAI and ζ :

$$K(\theta_v) = \exp(-LAI.\zeta(\theta_l, \theta_v))$$

LAI and average leaf inclination angle are initialized to the values computed by LAI2000 computation. The gap fraction for the five LAI2000 view angles is then computed with those values and compared to the measured gap

fraction. While the error between the estimation and the measure is too high, *LAI* and mean leaf inclination angle values are modified using the simplex optimization method. The cost function corresponds to the relative root mean square error (*RRMSE*) between the measured transmittance in the five view angles and the modelled one, with a constraint on *LAI* (if *LAI* higher than 9, the cost function is drastically increasing) and *ALA* (between 0° and 90°). We used the simplex algorithm available in the matlab optimization toolbox.

3. Look-up table

A look-up table containing 50000 elements is built using the same model as in §b, considering uniform distributions of *LAI* (between 0 and 8) and *ALA* (between 0° and 90°). Each LUT element corresponds to one (*LAI*, *ALA*) value and the corresponding gap fraction in the five rings. The *RRMSE* between the measured transmittance in the five view angles and each LUT element is computed. We then select the 25 elements with the lowest *RRMSE* and take the median value.

4. Results

Figure 4 presents the results we obtained using the three LAI and ALA computation methods. For LAI, discrepancies are observed between the optimization method and the two others although the initial guess of the solution is given by the LAI2000 computation. This demonstrates that the optimization method using constraints is quite sensitive to local minima. Differences between LUT and LAI2000 are decreased when considering an average LAI value for each field (Figure 4.b). However, for ALA, high discrepancies are observed between the three methods. This is mainly due to the lack of information on the monodirectional gap fraction, since only five view angles are available to perform the inversion.

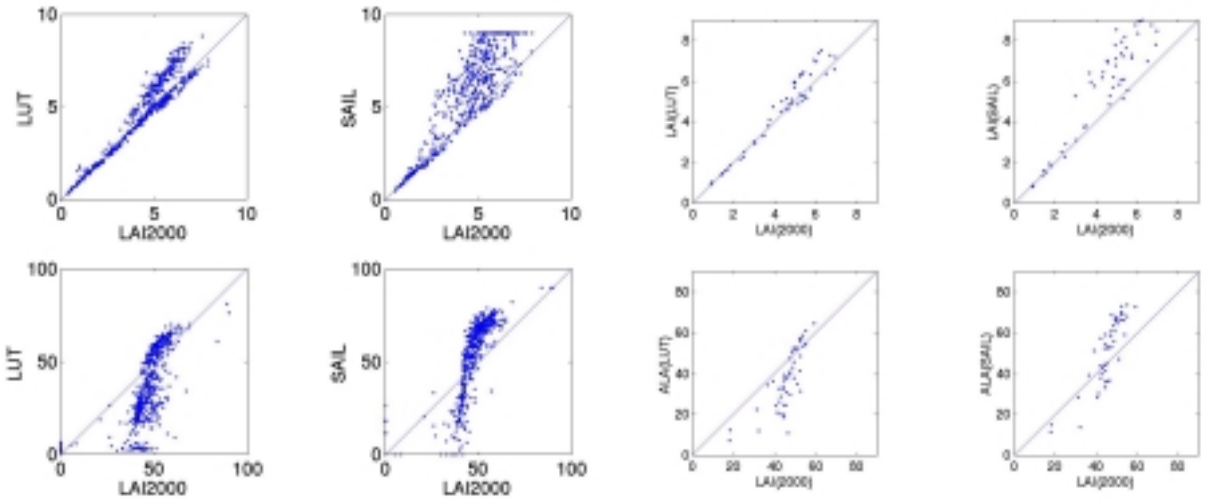

(a) (b)

Figure 4. Comparison between the 3 LAI computation methods. (a) considering each measurement point, (b) considering each field (average value)/

E. Hemiview Data processing

Hemispherical images have been acquired in fields where the vegetation was too low to use the LAI2000 instrument. A software developed at INRA (Zago, 2000) has been used to derive the monodirectional gap fraction in 19 zenith angles from 0° to 70° from the jpeg hemispherical pictures. Two kinds of masks are first applied to the hemispherical images in order to hide the operator's legs as well as the sky. Then, the masked image is binarized with zeros corresponding to vegetation pixels and 1 corresponding to bare soil, which allow to compute the monodirectional gap fraction. The leaf area index and average leaf inclination angle are then derived using the same process as in § D.2.

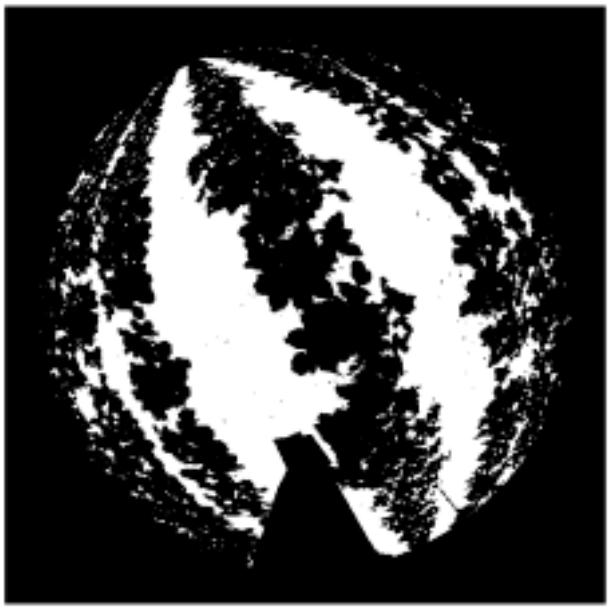

Figure 5. Example of processed image including masks and binarization (filed potato 5)

F. Atmospheric data processing

1. Aerosol optical thickness

- Except aerosol optical thickness, atmospheric parameters have been provided by Meteo France at the SPOT1 acquisition date, during the ground measurement campaign (Table 4).

Air Pressure (hPA at sea level)	1015.9	ARPEGE model
Water vapor content (gcm^{-2})	1.66	ARPEGE model
Ozone content ($atmcm^{-1}$)	0.306	TOVS/NOAA

Table 5: Atmospheric characteristics at Romilly site (06/08/2000). Meteo France data

- Total atmospheric optical thickness evaluation was achieved using a CIMEL sun-photometer, in 5 10nm-width wavebands (440nm, 670nm, 870nm, 936nm, 940nm), and a 50nm-width one at 1020nm on June, 8th 2000 (day 160). Acquisitions were performed from sunrise to sunset in very clear conditions, except early in the morning (haze). The temporal repetitivity of the measurements was 1mn at beginning and end, and about 30mn at midday. The symmetry with respect to 12HTU is well respected and gives good confidence in the measurements (Figure 6).

To derive the optical thickness τ_λ in each waveband λ, we used the Langley-Bouguer method (Wu et al., 1997). The direct monochromatic solar radiance measured by the sun-photometer can be expressed as:

$$\ln(V_l) - \ln(D_s) = \ln(kE_{o\lambda}) - \tau_\lambda m \qquad \text{Eq. 1}$$

where

- V_λ is the sun-photometer output
- D_s is the Sun-Earth distance, function of the day of the year J: $D_s = \left(1 - 0.01673 \cos\left|0.9856(J-4)\frac{\pi}{180}\right|\right)^{-1}$
- $kE_{0\lambda}$ is the mean solar irradiance outside the atmosphere times the instrument radiometric calibration coefficient (k).
- m is the mass number, function of the sun zenith angle θ_s and air pressure P: $m = \frac{P}{1013}\left(\cos\theta_s + 0.15(93.885 - \theta_s)^{-1.253}\right)^{-1}$

τ_λ can thus be deduced by linear regression between sun-photometer output minus D_s and air mass number. Data corresponding to sun zenith angles higher than 84° (m higher than 9.4) were removed due to problems with tracking the sun. As stated earlier, we have good consistency between morning and afternoon data (Figure 7).

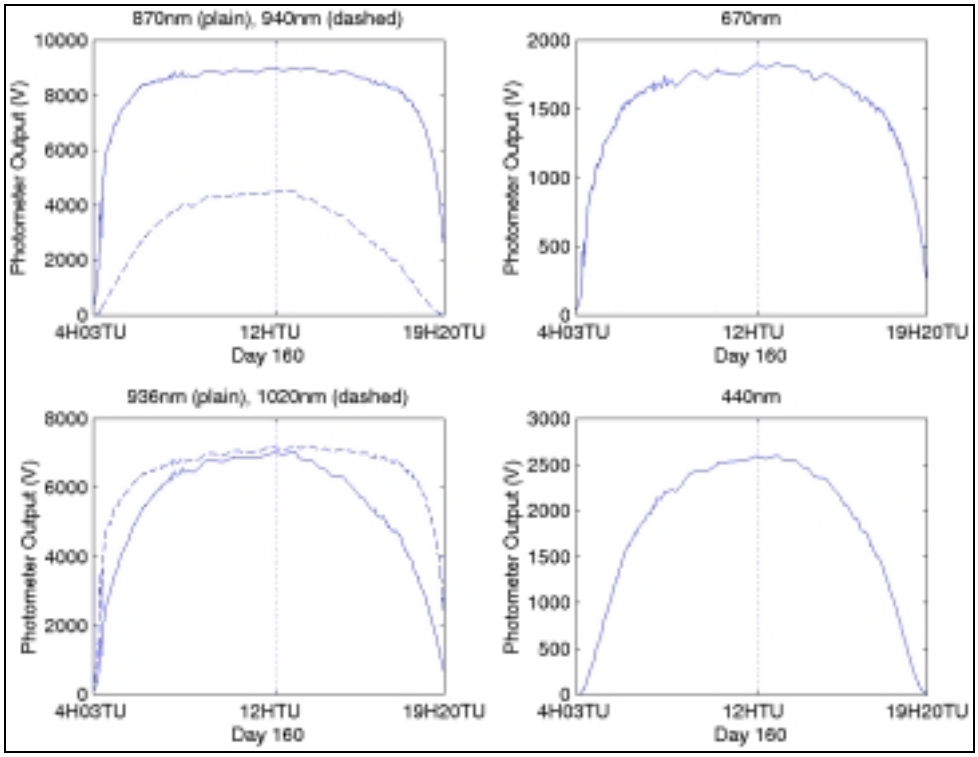

Figure 6. Sun-photometer measurements (Volts) as a function of time, in the six wavebands.

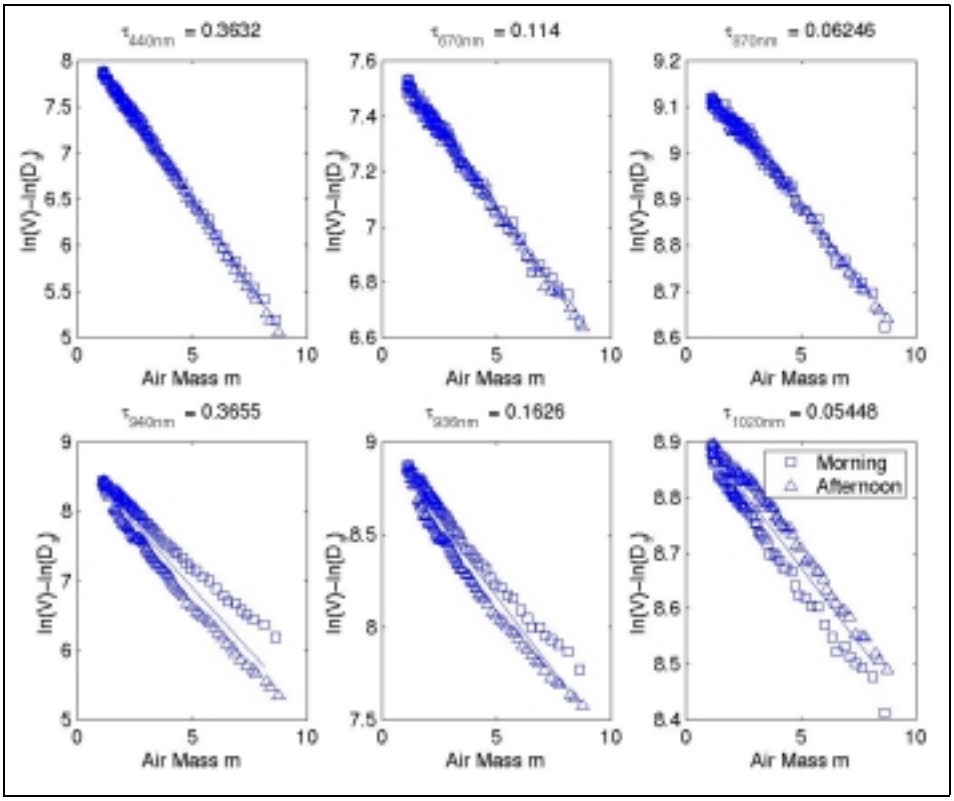

Figure 7. Linear regression between sun-photometer output and aerosol optical thickness in the 6 CIMEL wavebands.

- The aerosol optical thickness τ_{λ}^{aer} can then be derived:

$$\tau_\lambda^{aer} = \tau_\lambda - \left(\tau_\lambda^{ray} + \tau_\lambda^{gas}\right) \quad \text{Eq. 2}$$

where

- τ_λ^{ray} is the optical depth due to Rayleigh scattering of gas molecules. It is computed using table 5 and the 6S atmospheric model (Vermote et al., 1997).
- τ_λ^{gas} is the optical depth due to gas absorption. 6S was run for each wavelength and each solar position during the measurements to compute the total gaseous transmission ($T_g = e^{-m\tau_\lambda^{gas}}$, Figure 8).

	τ_λ^{aer}	τ_λ^{gas}	τ_λ^{ray}	τ_λ
440nm	0.1189	0.0007	0.2436	0.3632
670nm	0.0559	0.0144	0.0437	0.1140
870nm	0.0473	0.00005	0.0152	0.0625
936nm	0.1649	0.1892	0.0114	0.3655
940nm	-0.0071	0.1585	0.0112	0.1626
1020nm	0.0436	0.0028	0.0081	0.0545

Table 6. Optical depths computed from CIMEL measurements and the 6S model for the 8th June, 2000 on the Romilly site.

Significant values of gaseous optical depth are observed at 670nm due to ozone absorption, and at 936nm and 940nm due to strong water absorption. In those two last bands, the aerosol optical thickness derived from the CIMEL measurements is not realistic since aerosol influence decreases as the wavelength increases. The main cause is that the atmospheric water (as well as ozone) content may vary from the beginning to the end of the day, which explains the discrepancies between morning and afternoon in figure 7. Moreover, atmospheric characteristics provided by Meteo France were acquired at the nearest meteorologic station from Romilly site.

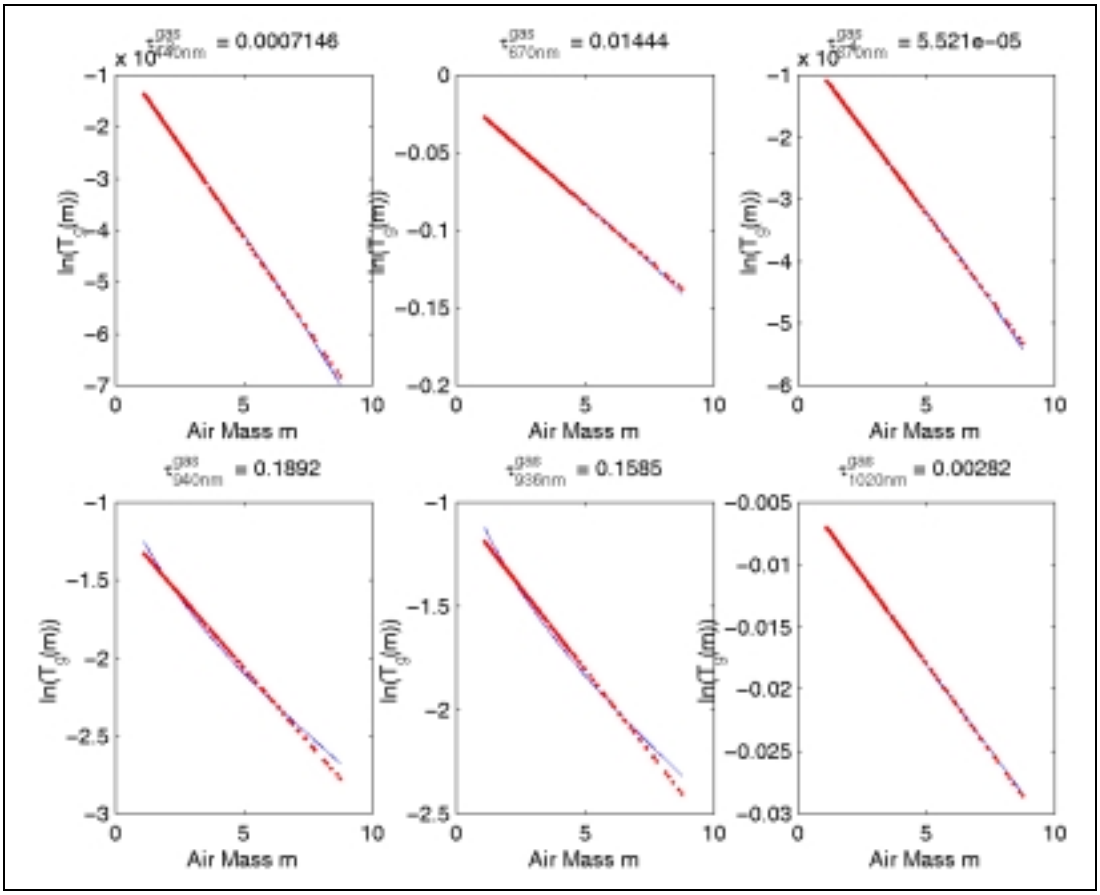

Figure 8. Evaluation of gaseous optical depth for each CIMEL waveband, using the 6S gaseous transmission computation and table 4.

To compute the aerosol optical thickness at 550nm, we used the Ångström law (Faizoun et al., 1994), which express the spectral dependence of the aerosol optical thickness as:

$$\tau_{\lambda}^{aer} = \beta\lambda^{-\alpha} \qquad \text{Eq. 3}$$

β is the aerosol optical thickness at 1μm, and α is the Ångström exponent , related to the particle size distribution. They are evaluated by linearizing and solving Eq. 3 using least square minimization, and the first three wavebands for which aerosol optical thickness is significant and there is only little gaseous absorption (ozone). Results gave $\alpha = 1.394$ and β=555.6 (wavelength in nm). The aerosol optical thickness at 550nm is deduced from Eq 3 using those coeffcients:

$$\tau_{550nm}^{aer} = 0.0841 \qquad \text{Eq. 4}$$

2. Diffuse and global radiation

Measurements of global and diffuse radiation were performed using two pyranometers (Kipp and Zonen CM6B) from day 146 to day 187, near the town of Provins (48°33'N, 3°18' W). This should allow to derive the total optical thickness for any day during this period, using the relationship found by Gu, during the Alpilles-ReSeDA campaign (personal communication):

$$R_{dir} = 1267\exp(-08\tau_{550nm}) - 100 \quad \left(\mathrm{Wm}^{-2}\right) \qquad \text{Eq. 5}$$

where $R_{dir} = R_g - R_{diff}$ is the direct solar radiation.

Measurements for day 160 confirm very clear day for sun photometer acquisition date (Figure 9a). The optical thickness deduced from these measurements using Eq 5 is shown in figure 9b. Eq 5 may be valid only between 11AM and 13PM since it was established and validated during the ReSeDA campaign for airborne measurements which took place during that time range. Results then give τ_{550nm}=0.31. Using the 6S model, we have evaluated the Rayleigh $\left(\tau_{550nm}^{ray} = 0.097\right)$ and gaseous $\left(\tau_{550nm}^{gaz} = 0.0053\right)$ contributions. This leads to an aerosol optical thickness at 550nm equal to 0.016, which is twice the results obtained by sun photometer measurements.

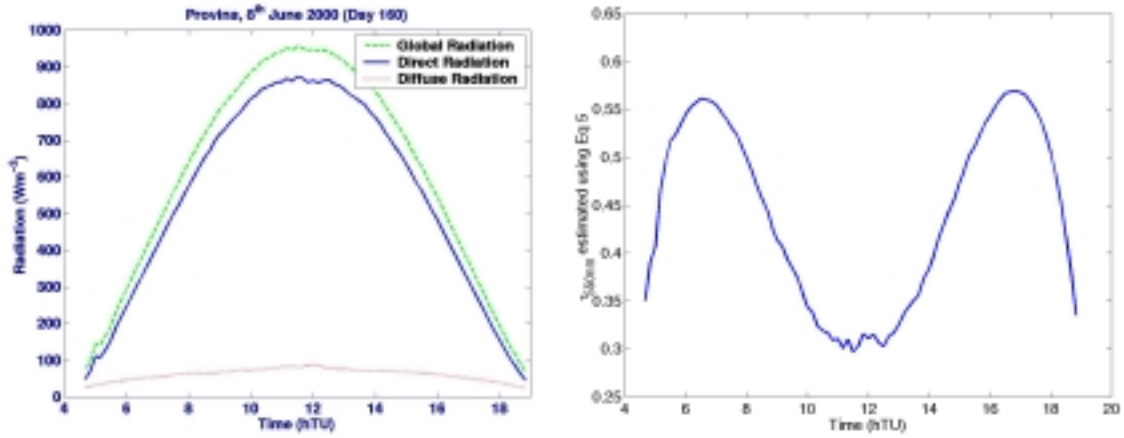

(a) (b)

Figure 9. (a). Global and diffuse radiation measured on day 160. (b). Total optical thickness at 550nm deduced from Eq 5.

3. Conclusions on aerosol optical thickness

High discrepancies are observed between the two methods of estimation. However, the value computed with the direct/diffuse radiation measurements is more realistic. In the near future, the manual sun photmeter will be calibrated using comparison with the automatic sun photometer from the AERONET network based at INRA, Avignon (France). There is also some need to go further in the validation of the relationship between optical thickness at 550nm and direct radiation.

G. Processed file format

LAI2000:

Column 1: Field Name
Column 2: Julian day of measurement
Column 3: Number of plots (N)
Column 4: East Lambert I Coordinate

Column 5: North Lambert I Coordinate
Column 6: Plot Number
Column 7: Gap Fraction for ring 1 (7°)
Column 8: Gap Fraction for ring 2 (23°)
Column 9: Gap Fraction for ring 3 (38°)
Column 10: Gap Fraction for ring 4 (53°)
Column 11: Gap Fraction for ring 5 (68°)
Column 12: Mean LAI (LAI2000 Computation)
Column 13: Mean LAI (SAIL Computation)
Column 14: Mean ALA (LAI2000 Computation)
Column 15: Mean ALA (LUT Computation)
Column 16: Mean ALA (SAIL Computation)

Hemiview

Column 1 : Field Name
Column 2 : Julian Day of measurement
Column 3 : Number of plots (N)
Column 4 : East Lambert I Coordinate
Column 5 : North Lambert I Coordinate
Column 6 : Plot Number
Column 7 : Gap Fraction for ring 1 (0°)
Column 8 : Gap Fraction for ring 2 (7.5°)
Column 9 : Gap Fraction for ring 3 (15°)
Column 10 : Gap Fraction for ring 4 (22.5°)
Column 11 : Gap Fraction for ring 5 (30°)
Column 12 : Gap Fraction for ring 6 (37.5°)
Column 13 : Gap Fraction for ring 7 (45°)
Column 14 : Gap Fraction for ring 8 (52.5°)
Column 15 : Gap Fraction for ring 9 (60°)
Column 16 : Gap Fraction for ring 10 (67.5°)
Column 17 : Mean LAI (SAIL Computation
Column 18 : Mean ALA (SAIl Computation)

When gap fraction in one direction is not available due to the mask applied to image, a NaN value is attributed.

RomillySunPhoto160.dat

Column 1 : Hour (TU)
Column 2 : Minute
Column 3 : Second
Column 4 : 440nm
Column 5 : 670nm
Column 6 : 870nm
Column 7 : 940nm
Column 8 : 936nm
Column 9 : 1020nm

Romilly_RgRdir.dat

Column 1 : Day of the year
Column 2 : Time (day+hour/24)
Column 3 : Hour (TU)
Column 4 : Global radiation
Column 5 : Diffuse radiation

H. References

Campbell, G.S., 1986. Extinction coefficients for radiation in plant canopies calculated using an ellipsoïdal inclination angle distribution. Agric. For. Meteorol., 36: 317-321.

Faizoun, C.A., Podaire, A. and Dedieu, G., 1994. Monitoring of Sahelian aerosol and atmospheric water vapor content characteristics from the sun photometer measurements. J. App. Meteor., 33(11): 1291-1303.

Lang, A.R.G., 1986. Leaf area and average leaf angle from direct transmission of sunlight. Aust. J. Bot., 34: 349-355.
Vermote, E.F., Tanré, D., Deuzé, J.L., Herman, M. and Morcrette, J.J., 1997. Second simulation of the satellite signal in the solar spectrum, 6S: an overview. IEEE Trans. Geosc. Remote Sens., 35(3): 675-686.
Welles, J.M. and Norman, J.M., 1991. Instrument for indirect measurement of canopy architecture. Agronomy Journal, 83(5): 818-825.
Wu, D. et al., 1997. Radiometric caracterization of Dunhang satellite calibration test site. In: G. Guyot and T. Phulpin (Editors), 7th International Symposium on Physical Measurements and Signatures in Remote Sensing, Courchevel, France.
Zago, M., 2000. Mesure des fractions de trou mono et bidirectionnelle de la végétation à partir d'images hémisphériques numériques., Université de Grenoble.